eprints@whiterose.ac.uk
https://eprints.whiterose.ac.uk/

4 **Multilayer nanoscale encapsulation of biofunctional peptides to enhance bone tissue**
5 **regeneration in vivo**
6

7 Piergiorgio Gentile*, Ana Marina Ferreira, Jill T Callaghan, Cheryl A Miller, Joss Atkinson,
8 Christine Freeman and Paul V Hatton*
9
10 Dr P. Gentile, Dr A.M. Ferreira
11 School of Mechanical and Systems Engineering
12 Newcastle University
13 Claremont Road
14 Newcastle upon Tyne NE1 7RU, United Kingdom
15 E-mail: piergiorgio.gentile@ncl.ac.uk
16
17
18 Dr J.T. Callaghan, Dr C.A. Miller, Mr Joss Atkinson, Mrs C. Freeman, Prof P.V. Hatton
19 School of Clinical Dentistry
20 University of Sheffield
21 19 Claremont Crescent
22 Sheffield S10 2TA, United Kingdom
23 E-mail: paul.hatton@sheffield.ac.uk
24

28 **Abstract text**

29 Bone tissue healing is a dynamic process that is initiated by the recruitment of osteoprogenitor

30 cells followed by their migration, proliferation, differentiation and development of a

31 mineralising extracellular matrix. The work aimed to manufacture a functionalised porous

32 membrane that stimulated early events in bone healing for initiating a regenerative cascade.

33 Layer-by-layer (LbL) assembly was proposed to modify the surface of osteoconductive

34 electrospun meshes, based on poly(lactic-co-glycolic acid) and nanohydroxyapatite, by using

35 poly(allylamine hydrochloride) and poly(sodium4-styrenesulfonate) as polyelectrolytes.

36 Molecular cues were incorporated by grafting peptide fragments into the discrete nanolayers.

37 KRSR sequence was grafted to enhance cell adhesion and proliferation,

38 NSPVNSKIPKACCVPTELSAI to guide bone marrow mesenchymal stem cells

39 differentiation in osteoblasts, and FHRRIKA to improve mineralisation matrix formation.

40   Scanning electron microscopy, infrared and X-Ray photoelectron spectroscopy demonstrated

41   the successful surface functionalisation. Furthermore, the peptides incorporation enhanced

42   cellular processes, with good viability and significant increase of alkaline phosphatase activity,

43   osteopontin and osteocalcin. The functionalised membrane induced a favourable in vivo

44   response after implantation for four weeks in non-healing rat calvarial defect model. It was

45   concluded that the multilayer nanoencapsulation of biofunctional peptides using LbL

46   approach has significant potential as innovative manufacturing technique to improve bone

47   regeneration in orthopaedic and craniofacial medical devices.

48

49 **Introduction**

50 Biomimetic scaffolds are ideal for bone regeneration due to their ability to mimic the native

51 extracellular matrix environment by incorporating biomolecules such as extracellular matrix

52 (ECM) proteins or short peptide fragments via surface modification or bulk incorporation.

53 They have the potential to interact with cells, promoting desirable cellular activities, i.e.

54 adhesion, proliferation, and differentiation [1]. Bone morphogenetic proteins (BMPs) are the

55 largely used growth factors involved in the improvement of bone regeneration [2], showing

56 their potential to differentiate mesenchymal stem cells into osteogenic cells [3]. However there

57 are a number of issues surrounding the use of full proteins in the body, that include: folding

58 randomly, dose, price, susceptibility to degradation, immunogenicity and purification [4].

59 Therefore, short peptides chain represents a viable alternative to these problems related with

60 full protein use and can reciprocate the signalling and binding domains of the long chain

61 proteins. Short peptides are characterised by reduced manufacturing cost and purification time

62 as well as they are much more stable and resistant than long protein to pH and thermal

63 changes [5]. Since the discovery of the arginine-glycine-aspartic acid (RGD) sequence in

64 fibronectin 30 years ago [6], there has been a vast array of proteins found in bone with high

65 number of cellular interactions possible through the different cell adhesion receptors.

66 Recently, Gentile et al. proposed two identified peptide fragments, FHRRIKA (phenylalanine-

67 histidine-arginine-arginine-isoleucine-lysine-alanine) and KRSR (lysine-arginine-serine-

68 arginine) for grafting scaffolds surfaces for bone regeneration [7]. It has been reported in

69 literature that KRSR sequence, identified in different adhesive proteins related with bone (i.e.

70 fibronectin, vitronectin, bone sialoprotein) is suitable for enhancing the osteoblast adhesion to

71 scaffold surfaces. [8] Dee et al. have demonstrated a comparable adhesion of osteoblasts on

72 surfaces modified by incorporation of KRSR and RGD [9].

73 Furthermore, several studies described that FHRRIKA sequence, derived from bone

74 sialoprotein, supported the matrix mineralisation [10]. Interestingly, as reported by Schuler

3

75 RGD combined with FHRRIKA or KRSR caused an improved osteoblast activities [11]. Other

76 short peptide fragments proposed in literature for bone regeneration are the hexapeptide

77 fragment GFOGER, extracted from collagen (type I), that stimulates the differentiation of

78 osteoblasts [12, 13] and the C-terminal pentapeptide YGFGG, derived from the osteogenic

79 growth peptide ALKRQRTLYGFGG, corresponding to the C-terminal of histone H4, able to

80 stimulate the proliferation and alkaline phosphatase activity (ALP) of MC3T3 osteoblastic-

81 like cells [13]. Finally the long peptide sequences, such as NSPVNSKIPKACCVPTELSAI

82 derived from BMP2, showed their potential to induce osteogenesis in vivo [13, 14]. However,

83 the overall number of peptide fragments used in bone can increase by using combinations of

84 the bone peptide sequences. The interactions between peptides or peptide combinations and

85 cells are not yet fully understood.

86 The most established methods proposed in the literature are to graft short peptide sequences

87 by adsorption [15] or chemical grafting (by click-chemistry or carbodiimide) [16]. Although,

88 traditional chemistry has been widely used to functionalise constructs with peptides, it does

89 not allow creation of 3D gradient peptide structures. In this work we propose an alternative

90 method, called layer-by-layer (LbL) assembly to build up peptide gradients in order to

91 modulate at nanoscale cellular response and induce faster bone formation. LbL technique is

92 based on the alternating exposure of positively and negatively solutions of charged polymers

93 called polyelectrolytes (PEs). It is an inexpensive, aqueous, conformal method for the creation

94 of nanolayered coatings with custom-made composition and structure, showing a large range

95 of optical, electrical, and biological properties [17, 18, 19]. Due to its versatility and simplicity for

96 incorporating high loadings of different types of biomolecules with a fine control over

97 multilayers structure, LbL provides a rational method towards the control of specific

98 biological activities. Recently, Zhou et al. prepared electrospun mesh, based on cellulose

99 acetate, modified by LbL in order to enhance antibacterial and antioxidative properties. Silver

100 nanoparticles-lysozyme compound and tannic acid $(AgNPs–Lys/TA)_n$ were used as a formula

101 to obtain the multilayered coating, where n was the number of the AgNPs–Lys/TA bilayers.

102 The outermost layer was Lys composite when n equalled to 5.5 and 10.5. These mats revealed

103 to be suitable in the areas of food packing, tissue engineering and wound dressing [20].

104 Moreover, Layer-by-Layer has been used to investigate the in situ differentiation of

105 mesenchymal stem cells (MSCs) into mature osteoblasts on titanium films, by using chitosan

106 and plasmid DNA (pEGFP–hBMP2) as polyelectrolytes. Compared with control groups,

107 MSCs cultured onto LbL-modified titanium films displayed higher production levels of

108 alkaline phosphatase and osteocalcin over 7 days and 14 days culture, respectively [21].

109 Therefore, LbL is highly attractive as a route to functionalise biomaterials or devices that

110 would otherwise be incapable of stimulating specific biological processes or enhanced healing.

111 While the research reviewed above has shown the potential for LbL to deliver small

112 molecules that retained their functionality, to date the stimulation of anabolic biological

113 processes by nanoencapsulated peptides has not been reported. In this work, we proposed the

114 LbL method to modify osteoconductive electrospun composite membranes (based on PLGA

115 and nano-hydroxyapatite) in order to impart a cascade of stimuli at the nanoscale and to

116 control the adhesion, proliferation and differentiation of mesenchymal stem cells, and the

117 formation of new bone matrix [22]. LbL allows to create a peptide gradient, where the cells,

118 according the dissolution of the multilayered coating, can interact subsequently with the

119 different peptide sequences (**Figure 1A-B**) for: (1) enhancing their adhesion, spreading and

120 proliferation (interaction with KRSR grafted on the top nanolayers), (2) guiding their

121 differentiation in osteoblasts (NSPVNSKIPKACCVPTELSAI grafted to the middle

122 nanolayers), and (3) improving the formation of mineralisation matrix (FHRRIKA on the

123 bottom nanolayers). The biocompatibility and osteogenic response has been evaluated in vitro

124 studying bone marrow mesenchymal stem cells differentiation in osteoblasts and in vivo using

125 non-healing rat calvarial defect model.

126   To summarise, it is the final aim of this work to manufacture a biomimetic construct using

127   LbL technology to simulate and so initiate a physiological bone healing cascade. If successful,

128   this approach could find wide application as a simple and reliable method to modify a wide

129   range of medical devices where stimulation of bone tissue regeneration was clinically

130   challenging and necessary.

131

132 **2. Results and Discussion**

133 A summary of the experiments is reported in **Figure 1**. The multilayered structure was

134 fabricated by Layer-by-Layer after accurate optimisation of the process parameters (**A**).

135 Specific bone peptides were grafted to the positive charged polyelectrolytes in order to mimic

136 the "bone healing" cascade (**B**). The osteogenic potential was measured in vitro after seeding

137 rat bone marrow mesenchymal stem cells (BM-MSCs) (**C**) on the membrane surface and in

138 vivo using a rat calvarial bone model (**D**).

139 In this work composite membranes, based on poly(lactic-co-glycolic acid) (PLGA) and

140 nanohydroxyapatite (nHA), have been obtained by electrospinning. This conventional method

141 has been widely accepted as the simple and less expensive method to fabricate random or

142 aligned fibrous matrices through the extrusion of the solution from a needle by an high

143 voltage electric field [23] By tuning electrospinning processing parameters it is possible to

144 modify fibres morphology and dimensions to enhance the spun morphology for promoting a

145 positive cellular response [24]. After optimisation of the process parameters (solution

146 concentration 20 %, voltage 20 kV, distance 18 cm and flow rate 2.5 mL/h) and smooth nano-

147 and micro- fibres were formed with the occurrence of some nHA aggregates, with a size

148 ranging from 800 nm to 1.4 µm (**Figure 2A**).

149 For mimicking the cascade of bone healing, the LbL approach has been used for obtaining a

150 multilayered coating on the electrospun membranes in order to graft appropriate bone peptide

151 sequences to the nanolayers (**Figure 1A**). Furthermore, 14 layers was chosen as final number

152 after optimisation of several process parameters: number of layers (10, 14 and 20 (**Figure**

153 **S1**)), dipping time into the PE solutions (10 and 15 minutes), polyelectrolytes molar

154 concentration (0.25 and 0.5 M), and bone peptide sequences grafting (several combinations

155 within the multilayers).

156 An optimised peptide gradient has been created after grafting to PAH: KRSR (from layer 10

157 to 14) to enhance cell adhesion, spreading and proliferation [11],

158   NSPVNSKIPKACCVPTELSAI (from layer 6 to 10) to guide BM-MSCs differentiation in

159   osteoblasts [12] and FHRRIKA (from layer 2 to 6) to improve the formation of mineralisation

160   matrix [11, 12]. Furthermore the small amount of peptide grafted on the PAH did not influence

161   the ζ-potential of the solution (+14.6 mV respect with +14.9 mV of pure PAH), while PSS

162   solution was always negatively charged with ζ-potential of -18.6 mV.

163   Finally, the presence of the osteoconductive nanohydroxyapatite in the electrospun mesh is

164   present to influence the cells to maintain the new osteoblast-like phenotype and guide their

165   growth along the fibre orientation [25]. The manufactured membranes were coded with the

166   corresponding number of the last layer created, following with "_P" if the bone peptide

167   sequences were grafted to PAH.

168   The surface morphology of the multilayered coating after LbL assembly was analysed by

169   Scanning Electron Microscopy (SEM) (**Figure 2B**). The membranes presented an average

170   fibres diameter of 1.7 ± 0.5 µm, without compromising the micro-porosity for nutrient

171   transport, making available biocues of the native ECM [26]. Successful immobilisation of

172   poly(sodium4-styrenesulfonate) (PSS) and poly(allylamine hydrochloride) (PAH) grafted

173   with peptides was monitored by several techniques although qualitative and semi-quantitative

174   information were provided. Specifically, Energy dispersive spectroscopy (EDS) proved the

175   formation of the multilayer coating by the difference in the amount of Sulphur and Nitrogen

176   (**Figure 3A** and **B**). For 14L_P membrane, S and N content was 8.8 ± 0.5 wt. % and 5.5 ± 0.3

177   wt. % considerable higher than the amounts detected in the uncoated mesh (0.1 wt. % for

178   sulphur and 0.5 wt. % for nitrogen). Furthermore, the maps (**Figure 3B (ii)**) evidenced a

179   uniform distribution of sulphur (pink dots) and nitrogen (green dots) on the membrane surface,

180   that was not observed for pure composite meshes, where calcium (red dots) and phosphorous

181   (blue dots) elements were present only (**Figure 3A (ii)**).

182   X-ray photoelectron (XPS) and infrared spectroscopy (ATR-FTIR) were performed to analyse

183   the surface composition of the membranes before and after LbL assembly. Particularly,

184 **Figure 4A** shows the XPS survey spectra after aminolysis treatment (PLGA/nHA_am) and

185 after the obtainment of 1, 4 and 14 layers. The surveys showed the characteristic S_{2p} peak at

186 168eV and N_{1s} peak at 399.5 eV, demonstrating PSS and PAH have been successfully

187 introduced.

188 The resulting atomic percentage of the main characteristic elements of the coating (C1s, O1s,

189 N1s and S2p) and the atomic ratio between S/N with the increase of layers number has been

190 calculated and reported in **Table 1**.

191 XPS confirmed again the realisation of the multilayer where the content of nitrogen and

192 sulphur increased. Moreover, the S/N atomic ratio had an alternating regular trend, suggesting

193 modifications in the surface chemical composition after LbL assembly. Particularly, S/N ratio

194 was higher with the PSS as top layer where sulphur was the representative chemical element

195 of PSS and nitrogen was for PAH. Similar results were observed previously by the same

196 authors, after functionalising PLGA dense film by LbL assembly (using the same PEs of the

197 current work) to impart antimicrobial activity after incorporation of an antibiotic drug [19].

198 Notwithstanding, the presence of the peptides was influencing slightly the values of nitrogen

199 content in the even layers, due to their low amount grafted to PAH (data not shown).

200 The high resolution spectra for C_{1s} along with the curve fit (**Figure 4B**) show three peaks

201 attributed to the different Carbon oxidation states: (1) 284.7−285.0, (2) 286.8−287.0, and (3)

202 288.5−289 eV, corresponding to −C−H or−C−C− bonds, to −C−O- bond [27], and to -N-C=O

203 (amide) groups [28] respectively. Moreover, from **Table 1** that summarises all the data, it is

204 observed that these components content varied significantly. The concentration of -N-C=O

205 (23.5±1.4% for the aminolysed sample) decreased drastically with the increase layer number

206 (4.2±1.1% for 14L_P). For the coated sample, the component at 284.7 eV corresponding to

207 C−C bonds increased reaching a final value of (83.0±2.3%) and the component at 286.9 eV

208 attributed to C−O bonds decreased reaching a final value of (11.8±1.2%), suggesting the PE

209 coating.

9

210   Furthermore the infrared spectra showed in **Figure 5A** revealed the presence of the

211   characteristic chemical bands of the polyelectrolytes: for poly(sodium4-styrenesulfonate): νO-

212   H stretching of the adsorbed water (frequency range 3700 - 3000 cm^{-1}), aromatic νC-H

213   stretching (3100 cm^{-1}); alkyl νC-H stretching (2920 cm^{-1}); aromatic δC-H bending (1800 and

214   1925 cm^{-1}); νO-H bending vibrations of absorbed water (1640 cm^{-1}), aromatic νC=C-

215   stretching (1600, 1500, 1450 and 1410 cm^{-1}), νSO$_3^-$ symmetric and asymmetric stretching

216   (1040-1005 cm^{-1} and 1190-1130 cm^{-1} respectively) [29].

217   Poly(allylamine hydrochloride was characterised by the following chemical bands: νN-H

218   stretching (3360 cm^{-1}); alkyl νC-H stretching (2920 cm^{-1}); N-H symmetric and asymmetric

219   scissoring vibrations (1490 cm^{-1} and 1580 cm^{-1} respectively), and νN-H asymmetric stretching

220   (1330 cm^{-1} [29]. Finally, the presence of the peptide grafting into nanolayered structure has

221   been indicated by the typical absorption peaks of the Amide I and II at 1650 and 1520 cm^{-1}

222   respectively) [30]. Amide A and III of the peptides typical bands were not clearly observed

223   because the polyelectrolytes bands caused an overlap.

224   In vitro dissolution tests has been performed for testing the coating stability. ATR-FTIR

225   spectra were obtained after 2, 4 and 6 weeks of immersion in Phosphate Buffer Saline (PBS).

226   **Figure 5B**-**D** shows that the intensity of the characteristic chemical bands of PSS, PAH and

227   peptide sequences decreased with the increase of immersion time. Particularly, after 2 and 4

228   weeks it was calculated a dissolution degree of ~35 and ~75 % respectively. Finally after 6

229   weeks it was noticed only weak absorption peaks of the corresponding polyelectrolytes,

230   suggesting a complete dissolution of the coating. The dissolution measured is in accordance

231   with the time required for the osteoblastogenesis in vitro [31].

232   The presented design of the functionalised membranes was proposed after combination of

233   several process variables and characterising not only by physico-chemical characterisation but

234   also by analysing cells behaviour (as reported in the supporting information section also). In

235   this study we used bone marrow-derived mesenchymal stem cells, the best characterised cells

236 to represent adult stem cell population capable of differentiation into various lineages [32]. The

237 BM-MSCs were extracted from rats according the protocol proposed by Santocildes-Romero

238 [33] and were seeded on uncoated and coated membranes.

239 Designing and manufacturing a biocompatible materials is one of the most challenging key

240 feature for the in vivo scaffold implantation. Therefore, several approaches have been

241 described in literature for modifying successfully the surface of scaffolds, such as by physical

242 absorption, encapsulation, chemical treatment, and ionic or covalent binding.[34] However the

243 encapsulation and physical absorption are characterised by weak biomolecules stability due to

244 their fast release when the functionalised scaffolds are implanted in vivo for a medium and

245 long-term. In addition, the entrapped biomolecules present poor resistance to shear stress of

246 the fluids. [34] The LbL assembly is a versatile and environmental-friendly method, widely

247 used in many fields, that allows the immobilization of different biomolecules to impart

248 specific biological activities. Moreover, in this work the covalent immobilization of bone

249 peptide sequences permits to avoid the removal of the grafted biomolecules by washing [18].

250 Biocompatibility tests were performed to evaluate whether the polyelectrolytes and the

251 grafting between PAH and peptide sequences affected the BM-MSCs viability and

252 proliferation. PrestoBlue® analysis (**Figure 6A**) showed that BM-MSCs in both coated

253 membranes with and without peptides exhibited a metabolic activity higher comparable with

254 the control after 3 and 7 days. In the case of 14L_P sample, the cells displayed a significant

255 higher metabolic activity (i.e. after 7 days of cells seeding, normalised fluorescence units for

256 14L_P and 14L were 0.243 ± 0.021 and 0.152 ± 0.018).

257 Therefore, the addition of the peptide sequences affected dramatically the adhesion and

258 metabolic activity of BM-MSCs in a short term period, and particularly the authors found

259 40% more viability on membrane with KRSR grafted to the top layer in comparison with

260 FHRRIKA and NSPVNSKIPKACCVPTELSAI (see **Figure S2**). Sun et al. described also the

261 role of KRSR influence, where the MC3T3-E1 attachment and osteogenic differentiation was

262 improved significantly on the TiO_2 anodized nanotube-layers grafted with KRSR for

263 orthopaedic and dental implants applications.[35] Moreover, Schuler et al. reported that

264 scaffold surfaces modified with KRSR sequence preferred osteoblast-like cells in comparison

265 with fibroblasts or endothelial cells in terms of cell proliferation. [11]

266 It is commonly accepted that changes of Alkaline phosphatase activity in bone cells are

267 associated with a change of the differentiated state. Generally, an increase of ALP enzyme

268 activity is correlated with bone formation, increasing during the bone formation stage. [36] Not

269 surprisingly, the ALP quantification data (**Figure 6B**) showed significantly higher activity

270 levels when cells were cultured under osteogenic media rather than basal media. However, at

271 day 14 and 21 the levels of ALP activity on 14L_P under basal media cultures are

272 significantly higher than PLGA/nHA and 14L membranes (i.e. at day 21 under basal media

273 culture the grafting of the peptide significantly (* $p<0.05$) higher ALP activity levels

274 (0.046 ± 0.004) in respect to pure composite membrane (0.024 ± 0.003)). Although PLGA/nHA

275 and 14L membranes are not capable of inducing the ALP protein expression alone, they were

276 capable of improve the ALP expression during the differentiation process of BM-MSCs to

277 osteoblasts under osteogenic media condition for 21 days of culture.

278 In addition to the reported biological data, the differentiation level of BM-MSC under basal or

279 osteogenic media was assessed by quantitative expression of two major bone-specific proteins,

280 namely, osteopontin (OP) and osteocalcin (OC). The relative expression of those proteins was

281 normalised in respect to with the cell proliferation (**Figure 6C**-**D**). It is well described that

282 osteoblasts are differentiated cells that mineralise the bone matrix. OP that is synthesised by

283 bone forming cells, is a phosphoprotein, which has calcium-binding domains and is

284 responsible for cell attachment, proliferation, and ECM mineralization [37]. While OC, is a

285 bone-specific glycoprotein capable of binding with calcium, which promotes ECM

286 calcification [38]. Not surprisingly as described for ALP activity, the OP and OC evaluation

287 showed significantly higher protein expression levels when BM-MCSs were cultured under

288   osteogenic media rather than basal media [38]. In the case of OP, as expected, a delay in the

289   protein synthesis is observed (**Figure 6C**). At day 7 there was no significant difference in OP

290   expression in respect to the pure composite membrane under basal and osteogenic conditions.

291   However, at day 14 there is the highest expression peak for osteogenic media cultures, which

292   indicates the beginning of the mineralisation phase. Specifically, under osteogenic media all

293   the sample showed a significant (*$p<0.05$ for PLGA/nHA and 14L) and extremely significant

294   (**$p< 0.001$ for 14L_P) over-expression. To emphasise, all the samples under osteogenic

295   conditions and the 14L_P membrane under basal condition showed a significant

296   overexpression of OP protein at day 21, supporting the higher ALP activity. For OC

297   evaluation, there was a high protein expression up to day 14 (**Figure 6D**), indicating bone

298   ECM maturation. [39] At day 7 there is a significant difference of OC expression in respect to

299   the control (PLGA/nHA under basal medium conditions). PLGA/nHA and 14L_P membranes

300   showed the OC overexpression capacity at 14 and 21 days, representing significant

301   differences over the control. Notable is that 14L_P under basal media condition exhibited a

302   peak of expression at day 21, suggesting that this membrane was able to induce in long term

303   OC protein expression, which corroborates the ALP data.

304   Finally, preliminary in vivo tests using a rat calvarial model were performed. After 4 weeks of

305   implantation there was increased new bone formation when a construct was utilised compared

306   to sham operated sites with no construct (**Figure 7A, Movie S1**). MicroCT investigation

307   indicated that the volume percentage of new formed bone in the defect treated with

308   PLGA/nHA, 14L and 14L_P were 13.7±3.6%, 15.8±4.1% and 24.6±3.8%; thus all

309   membranes let to an improved healing in comparison with the subject matched empty defect

310   in which the volume percentages of new bone were 7.7±1.9%, 8.5±2.8% and 9.4±2.2%

311   respectively (**Figure 7B-D**, **Movie S2**, **S3** and **S4**). While these increases did not show

312   significant differences between the constructs it suggests that they could encourage bone

313   healing and that any significant difference between them was not evident at this single time

314   point. When compared to other studies reported in literature using pure membranes based on

315   PLGA/collagen/HA or collagen/HA, the volume percentage of new formed bone in the defect

316   treated with 14L_P was higher (~25% respect to ~6-10%) after 4 weeks of implantation [40].

317   Moreover, the trend in the formation of new bone was found also comparable with more

318   sophisticated membrane, described in literature, where a scaffold sheet of medical grade

319   polycaprolactone/tricalcium phosphate/collagen was functionalised with the addition of BMP-

320   2 and, then implanted in cranial model [41]. Sawyer et al. demonstrated that the addition of

321   bioactive molecules increased dramatically the new bone growth respect with the non-

322   functionalised composite membrane (from ~12 mm^3 to ~19 mm^3 of bone volume). Therefore,

323   the biomimetic approach of functionalising scaffolds with the addition of proper biomolecules

324   can be considered a promising and cheaper alternative to tissue engineered cell–polymer

325   constructs [42].

326   Histological assessment of the rat calvaria was performed on completion of micro-CT

327   examination. Haematoxylin and eosin-stained sections were examined using conventional

328   light microscopy. New bone was noted at the periphery and centre of the defects for 14L-P

329   sample (**Figure 7H**), as opposed to the other groups (**Figure 7F-G**, PLGA/nHA and 14L),

330   where new bone was restricted to the margins. The histological findings in terms of

331   distribution of new bone were consistent with the appearances noted on micro-CT and lend

332   support for the usefulness of this image modality in the assessment of bone response to novel

333   materials. All animals recovered well after surgery with no adverse events noted; the

334   membranes were biocompatible in the model used and were associated with improved bone

335   healing when compared with sham operated sites. An initial inflammatory infiltrate was noted

336   but given the presence of foreign material and wound healing this is to be expected and no

337   unusual features were noted. Further work would be required to evaluate membrane

338   degradation and long term tissue responses to the membranes, and the possibility to use the

339   proposed functionalised membrane as layer of a bi- or multi- phasic scaffold for bone tissue

340   engineering, as proposed by Ivanovski's group.[43]

341

342   **3. Conclusion**

343   We have demonstrated the utility of LbL to assemble structures characterised by tailored

344   morphological, chemical and biological features in tissue engineering. The advantages of this

345   low temperature nanoencapsulation technology are evident, as sensitive molecules may be

346   incorporated for predictable release without loss of biofunctionality. The LbL-modified

347   membrane was shown to be both more biocompatible and able to impart an increase in the

348   expression of the ALP activity and two major bone-specific proteins, osteopontin and

349   osteocalcin, compared with all control materials. The functionalised membrane reported here

350   is a substantial improvement on existing commercial devices on account of its degradability

351   and greatly enhanced osteoconductivity via direct interaction of the biomaterial surface with

352   cells in order to enhance tissue regeneration and healing. This is the first report of LbL being

353   employed successfully to encourage bone tissue regeneration in vivo. It was concluded that

354   the multilayer nanoscale encapsulation of biofunctional peptides using an LbL approach has

355   great potential as an innovative manufacturing process to substantially improve bone tissue

356   regeneration when using orthopaedic and craniofacial medical devices.

357

4. Experimental Section

Materials. Calcium hydroxide, phosphoric acid (85 wt%, >99% pure), docusate sodium salt (DSS), poly(D,L-lactide-co-glycolide) (PLGA; LA/GA ratio (75/25), Mw = 66-107 kDa), ε-maleimidocaproic acid (EMCA), N-(3-Dimethylaminopropyl)-N-ethylcarbodiimide hydrochloride (EDC), poly(sodium4-styrenesulfonate) (PSS average Mw = 70 kDa), N-Hydroxysuccinimide (NHS), and ethylenediamine (ED) were supplied from Sigma-Aldrich, UK. Poly(allylamine hydrochloride) (PAH) was supplied from Alfa Aesar, UK. The bone peptide sequences (N-acetyl-CFHRRIKA-amide, N-acetyl-CKRSR-amide and N-acetyl-NSPVNSKIPKACCVPTELSAI-amide) were synthesized (purity more than 95% by analytical HPLC) and supplied by Biomatik, Taiwan. Acetone (99.8%) was purchased from Fisher Scientific, UK. All materials and chemicals were used without further purification.

Electrospun membranes preparation. The electrospun membranes were prepared according the following protocol. A defined amount of nano-hydroxyapatite (nHA, 20-40 nm in width and 60-80 nm in length), synthesised according to the protocol described by the same authors [44], was dissolved in acetone (20% w/w respect with PLGA content) in ultrasonic bath stirring before the addition of the polymer. DSS surfactant (0.05% wt/v) was added to improve the stability of the nanoparticle suspension in the polymeric solution. Then PLGA (20% w/v) was added at 25 °C in order to obtain a composite solution. The electrospinning parameters were optimized and membranes were prepared with a static 21G needle and a flat paper plate to collect randomly oriented nanofibres. The solution was spinnable in the following conditions: distance from tip to the metallic collector of 18 cm, a flow of 2.5 ml/h, and an electric potential of 20 kV. The resulting membranes, coded as PLGA/nHA, were collected, left under hood overnight to remove solvent residues.

Aminolysis. Electrospun membranes were treated by aminolysis by dipping in ED solution (0.05 M) for 15 minutes at 20 °C for grafting $-NH_2-$ in order to get a positive charge on the surface. Then aminolysed meshes were washed five times in H_2O, dried under hood for 12 h.

384   Peptide conjugation. First step of the peptide conjugation was the maleimide groups grafting

385   to the poly(allylamine hydrochloride) sidechains: 1.5 mg of EMCA was added to 1 ml of

386   PAH solution (2 mg PAH, 23.7 mg EDC and 14.7 mg NHS) and left to react at 25 °C (room

387   temperature, RT) for 2 h. Gel filtration was performed in order to remove non-reacted

388   reactants and additional by-products. Then, the peptide sequences were grafted to PAH–g-

389   EMAC by reaction between of the maleimide group with the cysteine thiol groups. The molar

390   ratio between the maleimide groups and peptides was 2:3, and left to incubate at 4 °C for 24 h.

391   The peptide-g-PAH was coded as PAH-P.

392   LbL functionalisation. The assembly of PSS/PAH-P multilayers (shown in **Figure 1A**) was

393   performed at 25 °C. The polyelectrolytes were dissolved in order to obtain 5 mg/mL solutions

394   in 0.1 M NaCl with a pH of around 4.6. The ζ-potentials of the polyelectrolytes solutions was

395   measured by laser Doppler electrophoresis (Zetasizer Nano, Malvern instrument, USA).

396   Aminolysed membranes (size 5×5 cm and thickness ~ 180 µm) were dipped firstly in PSS

397   solution (5 mL) for 15 min. Then, they were washed in water containing 0.1 M NaCl at pH

398   4.6 for 5 min. The, the membranes were finally soaked in PAH-P solution (5 mL) for 15 min

399   followed with water washing step using the same parameters described before. This dipping

400   process was repeated for 7 cycles for creating 14 layers (7 bilayers of PSS/PAH-P) (**Figure**

401   **1B)**. Finally, the membranes were washed with distilled water for 10 min. The samples were

402   left to dry under hood overnight and stored in the fridge at 3 °C.

403   Physico-chemical characterisation. The morphological analysis of the samples before and

404   after LbL assembly was performed by Scanning electron microscopy (SEM, LEO 1450VP).

405   Membrane were coated with gold under vacuum (100 s) by Agar Auto Sputter Coater. The

406   diameters of the fibres and the pores were evaluated on at least five SEM micrographs using

407   ImageJ software. EDS analysis has been performed by using a bench SEM-equipped with

408   EDS (Hitachi TM3030). Surface composition of the membranes was analysed by XPS and

409   ATR-FTIR. XPS spectra were acquired on Theta Probe (Thermo Scientific, UK), equipped

410   with a microfocused AlKa X-ray source (1486.6 eV), operated with a 400 µm spot size (100

411   W power). Process parameters were: 200 eV pass energy, 1 eV step size of and of 50 ms

412   dwell time in not angle-resolved lens mode. At least 3 single area were evaluated on each

413   membrane surface. Moreover, high resolution spectra were acquired with 40 eV pass energy,

414   0.1 eV step size and 200 ms as dwell time.

415   ATR-FTIR spectra were acquired in a wavenumber range of 4000–550 cm^{-1} using a Nicolet

416   iS10 spectrometer (4 cm^{-1} resolution and 32 scans).

417   Dissolution in vitro tests were performed after immersion in 5 ml of Phosphate Buffer Saline

418   (PBS) solution at 37 °C for different time points (2, 4 and 6 weeks) with a PBS refresh every

419   2 days.

420   Cell tests. In vitro cell tests were performed on pure electrospun composite membranes, LbL

421   functionalised meshes without and with addition of peptides. Preliminary to the seeding of

422   cells, membranes (φ~ 1.2 cm diameter discs) were sterilised using UV light for 4 hours in 24-

423   well plates and rinsed five times with PBS. Rat Bone marrow stromal cells (BM-MSCs) were

424   grown in a controlled atmosphere (5 % CO_2 and T= 37 °C) in Iscove's modified Dulbecco's

425   medium (DMEM) supplemented with 10 % foetal calf serum (FCS, Sigma-Aldrich), 2 mM L-

426   glutamine (Sigma-Aldrich), penicillin (100 U/mL), and streptomycin (100 µg/mL; Sigma-

427   Aldrich) and 0.1 mM nonessential amino acids (NEAA, Lonza, UK) for 7 days. This medium

428   condition is considered as basal. For all experiments we used cells from up to two passages. A

429   number of 30,000 cells were seeded onto the samples in 1 ml DMEM.

430   After 3 and 7 days of cell culture, the medium was removed and the sample were transferred

431   to new 24-well plates; after addition of 10 % PrestoBlue solution (5 mg/mL in DMEM; Fisher

432   Scientific), the multiwell plates were kept in incubation for 1 h at 37 °C. After the supernatant

433   removal, the solution (now dark blue) was transferred in 96-well plates (0.2 mL) and

434   quantified spectrophotometrically at 560 nm (Leica DM2500). PicoGreen® dsDNA reagent

435   (Invitrogen, USA) was used to calculate the cell number for each sample in order to make a

436   correct normalisation of the fluorescence values. After each culturing period, the membranes

437   were washed with PBS and then incubated at 37 ºC for 3 h followed by freezing step at -80 ºC

438   for at least overnight in ultra-pure water (1 mL) to ensure cell lysis. The assay was performed

439   according to the manufacturer's protocol. And the fluorescence was determined at an

440   excitation wavelength of 485 nm and emission wavelength of 528 nm. The mean ± standard

441   deviation were calculated for five tests.

442   After 21 days of cell culture BM-MSCs differentiation was evaluated in basal (as described

443   before) and osteogenic medium (after 1 week of cell seeding consisted of basal medium plus

444   50 μg/mL ascorbic acid, 10^{-8} M dexamethasone (Sigma-Aldrich) and 10 mM β-

445   glycerophosphate (Fluka Biochemika)). Alkaline Phosphatase activity was evaluated after 7,

446   14 and 21 days by adding 500 μL alkaline buffer solution and 0.5 mL of stock substrate

447   solution (40 mg p-nitrophenyl phosphate disodium, Sigma-Aldrich) to 100 μL of each lysate

448   samples (obtained following the same protocol described for the PicoGreen assay), diluted in

449   10 mL of distilled H_2O for 1 h at 37 °C. The p-nitrophenol production was analysed by

450   monitoring the solution absorbance using Leica DM2500 at 410 nm. PicoGreen® dsDNA

451   reagent (Invitrogen, USA) was used to calculate the cell number for each sample in order to

452   make a correct normalisation of the ALP absorbance values. The mean ± standard deviation

453   were calculated for three tests.

454   Osteopontin (OP) and osteocalcin (OC) protein expression of BM-MSCs was assessed by

455   immunoassay technique to evaluate the osteoblast differentiation. The concentration of OP

456   and OC was determined for all time culture periods, using the lysates used for DNA

457   quantification by Picogreen. OP quantitative determination was performed by the use of

458   Mouse/Rat Osteopontin Quantikine ELISA Kit (R&D Systems, UK). In brief, 50 μL of assay

459   diluent RD1W and 50 μL of standard (2500 to 39 pg/mL), control and membrane were added

460   into to the multi-well plate and kept to incubate at 25 °C for 2 h. After 4 washing steps, 100

461   μL of Mouse/Rat OPN conjugated were added and incubated at 25 °C for 2 h. The sandwich

462 complex was rinsed 4 times in order to react with 100 µL of substrate solution before adding

463 100 µL of stop solution. Finally, the optical density was determined at 450 nm and

464 concentration of OP obtained from standard curve plot. OC quantitative determination was

465 performed by the use of Rat Bla-Osteocalcin High Sensitive EIA kit (Takara Clontech, Japan).

466 In brief, 100 µL of samples and standard solution (16 to 0.25 ng/mL) were incubated for 1 h

467 at 37 ℃ with the capture-antibody, rat osteocalcin C-terminus-specific antibody. After OC

468 capture and 3 washing steps, 100 µL of the enzyme-labelled antibody (GlaOC4-30) specific to

469 Gla-OC was incubated at room temperature for 1 h. The sandwich complex was rinsed 4

470 times and allowed to react with 100 µL of substrate solution for 10-15 min. Finally, after

471 adding the stop solution the optical density was determined at 450 nm and concentration of

472 OC obtained from standard curve plot. OP and OC content was calculated by normalising OP

473 or OC concentration per DNA concentration for each condition and time point.

474 In vivo tests. The potential of enhanced bone regeneration in vivo was assessed by

475 implantation of the constructs into 4.5 mm Ø defects created in the crania of adult male

476 Wistar rats (the average weight at the time of surgery was 320 g). The rats were assigned to

477 one of three experimental groups (PLGA/nHA, 14L and 14L_P) each of which comprised

478 three animals. General anaesthesia was induced and maintained using Isoflurane in oxygen;

479 after induction of anaesthesia a single dose of 0.05 ml Carprofen (Rimadyl™, Pfizer Ltd,

480 Sandwich, Kent, UK) was given by subcutaneous injection.

481 A midline incision was made over the cranial vault and the skin and periosteum reflected to

482 reveal the skull. A single circular defect 4.5mm diameter was made on each side of the

483 midline using a diamond tipped surgical bur with saline irrigation. A sample of test membrane

484 was placed over one defect and the other left untreated to act as an internal control. The

485 periosteum and skin were carefully repositioned to avoid moving the membrane and wounds

486 were closed with resorbable sutures (Vicryl™, Ethicon Ltd. Edinburgh, UK) and the animals

487 were allowed to recover before returning to clean cages.

488 Animals were housed in groups of three and preserved under standard laboratory conditions

489 with free access to food and water. Four weeks after surgery animals were sacrificed using a

490 schedule one method and the heads removed and placed in formalin for fixation prior to

491 processing for Micro-CT and histological processing. Specifically, trimmed specimens were

492 scanned using a desktop microtomograph (Sky Scan 1172, Aartselaar, Belgium) through 360°

493 at a setting 1 voxel = 10 µm. The voltage used was 70 kV, the current was 130 µA and the

494 aluminium filter was set at 0.5 mm. The scan was collected using the medium camera (2000

495 x 1048), 0.7 rotations with x2 averaging. Reconstruction was done using NRecon

496 (SkyScan1172, Aartselaar, Belgium) by correcting for ring artefacts and 15% for beam

497 hardening. The data was segmented and analysed in CT Analyser (Bruker software) using

498 threshold level 60 -255. The new bone formation was calculated as a percentage Bone

499 Volume / Tissue Volume (% BV/TV) in 4.5 mmØ x 0.7 mm depth within the defect. A 3D

500 image of each sample was created in CTvox (ver. 3 Sky scan Bruker) using the transfer

501 function 'Steph bone cortical.tf' (Dr. S Borg, University of Sheffield).

502 Trimmed specimens were decalcified and processed to produce Haematoxylin and Eosin

503 stained sections for conventional light microscopy; histological images were collected on

504 Aperio scan (Leica Microscopes UK ltd).

505 Statistical analysis. Tests were performed at least three times for each membrane. All data

506 were expressed as mean ± SD. Statistical analysis was determined by using Graph pad Prism

507 6 software. The statistical differences between groups were calculated using Kruskal-Wallis

508 One Way Analysis of Variance on Ranks (ANOVA). Statistical significance was declared at *

509 $p < 0.05$, ** $p < 0.001$ and *** $p < 0.0001$.

510 **Acknowledgements**

513   photoelectron spectra were obtained at the National EPSRC XPS User's Service (NEXUS) at

514   Newcastle University, a UK EPSRC Mid-Range Facility.

515

516

520

521 **Figures**

522 **Figure 1.** Schematic diagram of the manufacturing of nanofunctionalised electrospun
523 membranes and their application for mimicking bone healing repair and regeneration: **A.**
524 Layer-by-layer method with the alternating exposure of the pre-charged membrane in
525 polyelectrolytes solutions; **B.** Bone peptide sequences grafted to the positive-charged
526 polyelectrolyte; **C.** In vitro tests by seeding BM-MSCs on the electrospun nanofunctionalised
527 membranes; **D.** In vitro tests using non-healing defect (~4.5 mm) in a rat calvarial model.
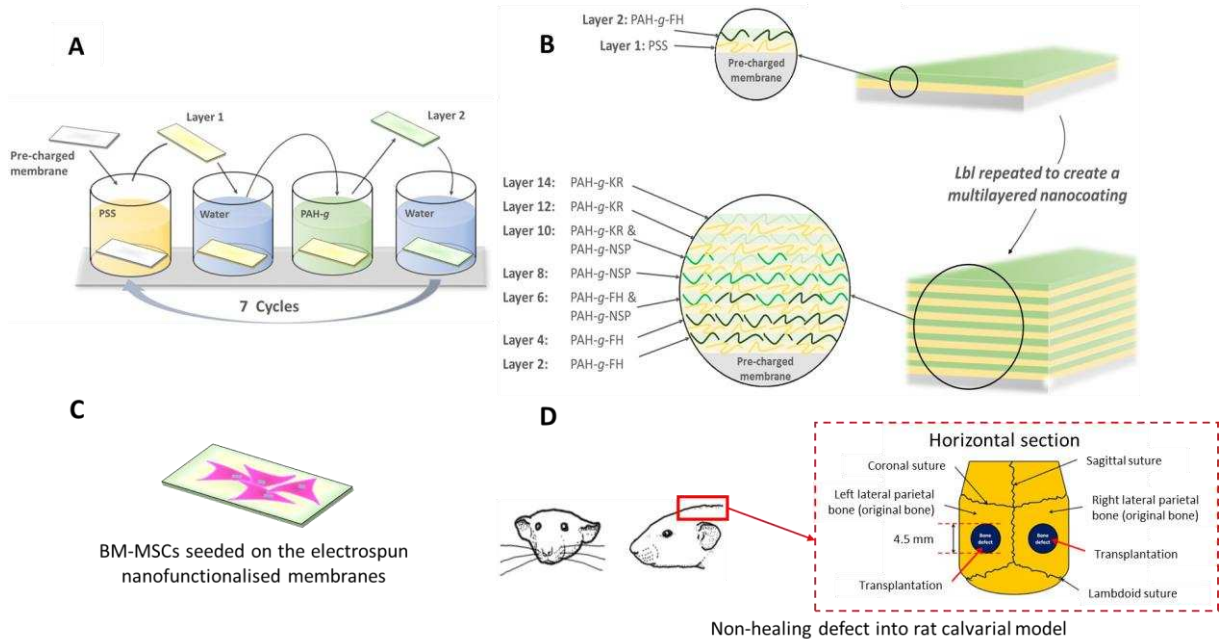
528

529

530 **Figure 2.** SEM micrographs of the electrospun membranes before and after Layer-by-layer
531 surface modification (bar= 5µm). The insets show the macrographs of the electrospun
532 membranes (Magnification 3000x, bar= 10mm).

533

534
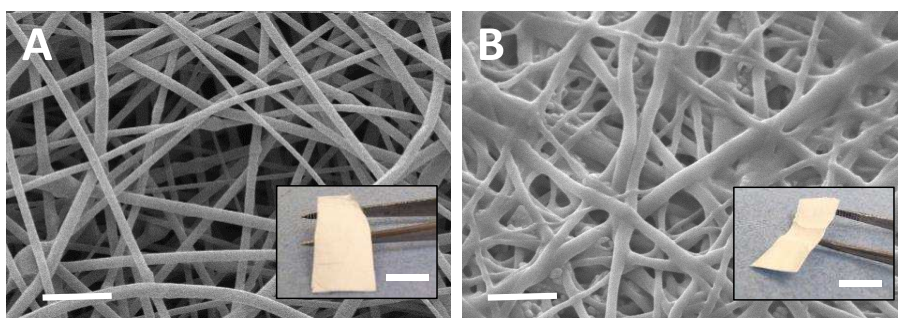
Figure 3. EDS analysis of the electrospun membranes before (**A**) and after Layer-by-layer surface modification (14L_P) (**B**), with the acquisition of the following outputs: (i) SEM micrograph, (ii) punctual elemental composition, and (iii) EDS spectrum. Bars = 50 µm.

25
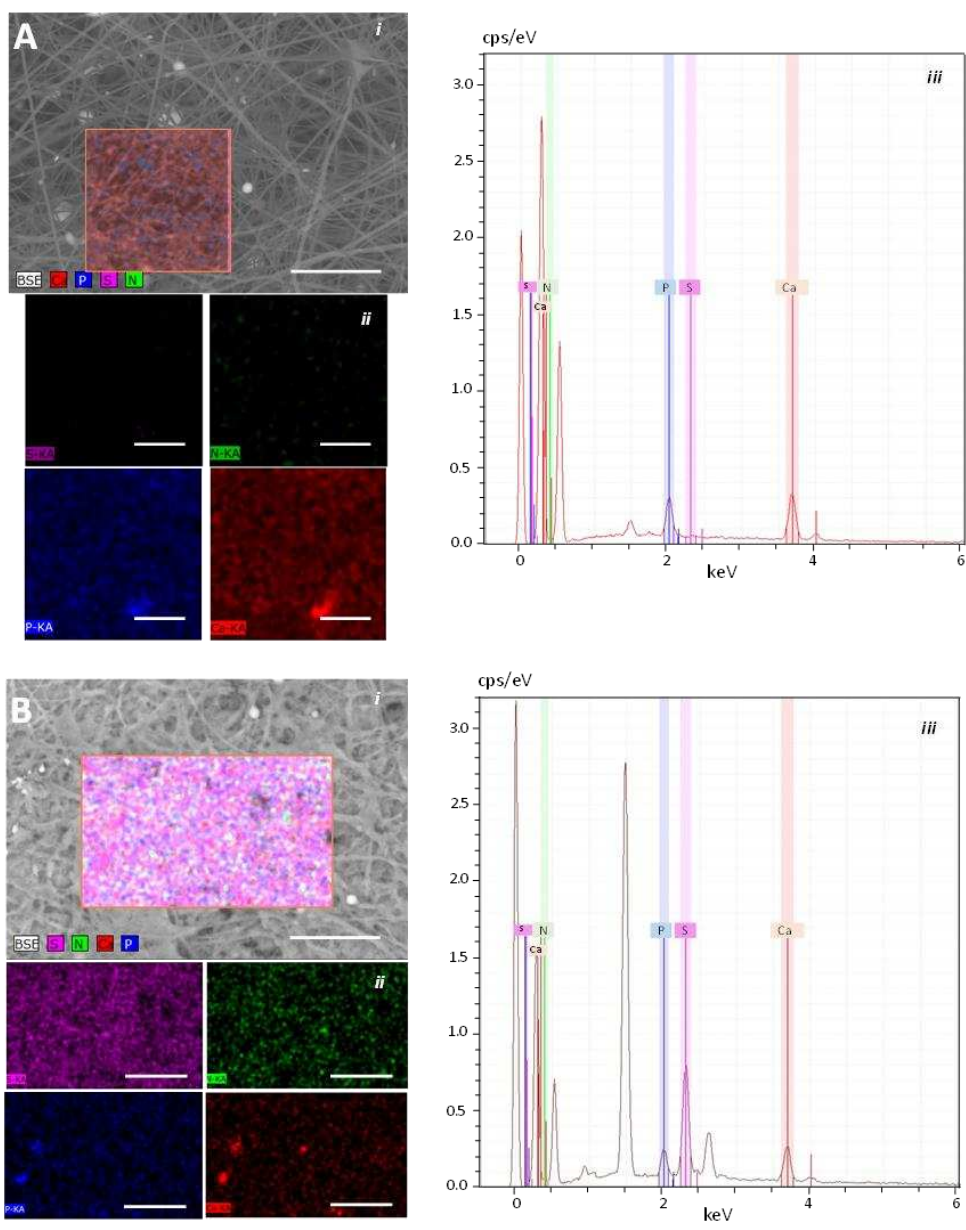
541 **Figure 4.** XPS spectra after functionalization by Layer-by-layer assembly. **A.** Survey spectra
542 and **B.** deconvoluted C1s spectra for pure composite membrane after aminolysis and after
543 coating of 1, 4 and 14 layers respectively.
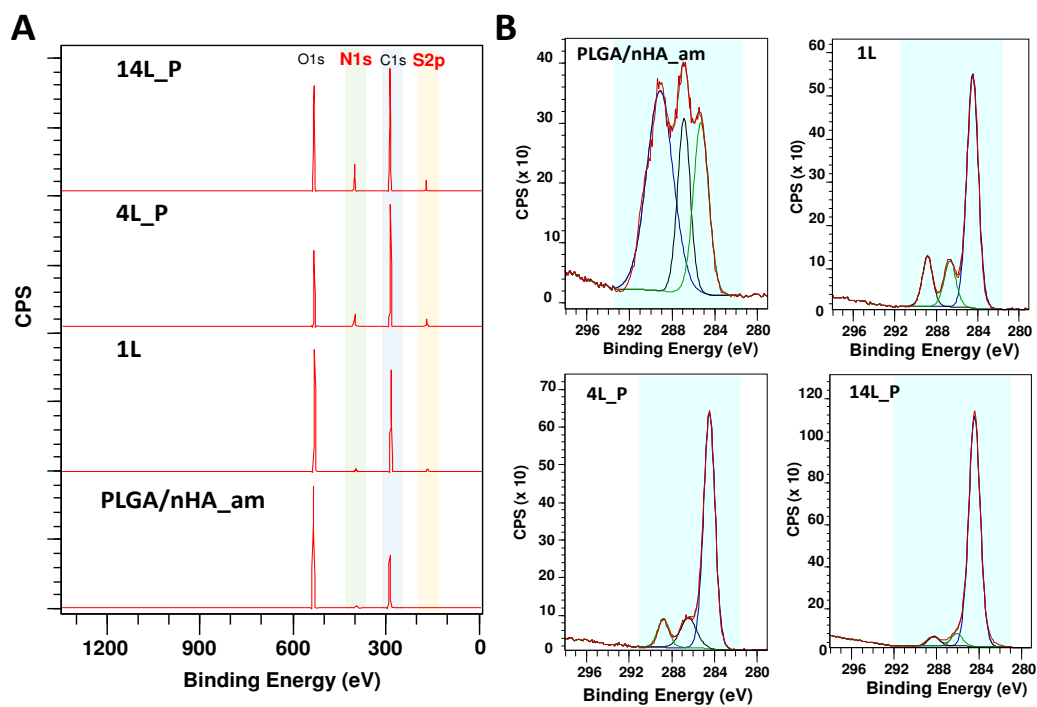
544

545

546 **Figure 5.** ATR-FTIR spectra of the Layer-by-layer functionalised electrospun membranes (**A**)
547 and after in vitro dissolution test in PBS at 2 weeks (**B**), 4 weeks (**C**) and 6 weeks (**D**)
548 (resolution 4 cm^{-1}; 32 scans). The most important peaks of the nanocoating are evidenced in a
549 coloured area: PSS in beige, PAH in green and the bone peptide sequences in blue colour
550 respectively.

551

552
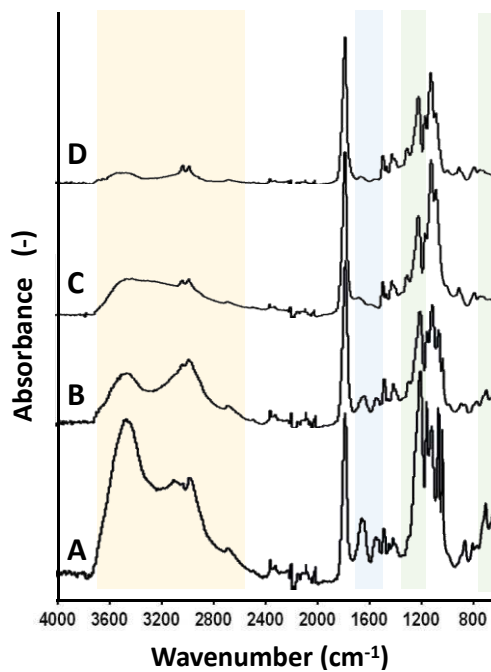
Figure 6. In vitro cell tests. **A.** BM-MSCs metabolic activity (PrestoBlue® assay) after culturing for 3 and 7 days. **B.** Intracellular alkaline phosphatase activity of BM-MSCs (Alkaline Phosphatase detection kit –Sigma Aldrich Alkaline phosphatase assay kit (APF-1KT)) after culturing either with basal or osteogenic media for 7, 14 and 21 days. **C.** Osteopontin protein content of BM-MSCs cultured either with basal or osteogenic media at 7, 14 and 21 days. **D.** Osteocalcin protein content of BM-MSCs cultured either with basal or osteogenic media at 7, 14 and 21 days. The statistic significance is in respect to the control of PLGA membrane in basal media for each time point (* $p<0.05$, ** $p< 0.001$ and *** $p< 0.0001$).
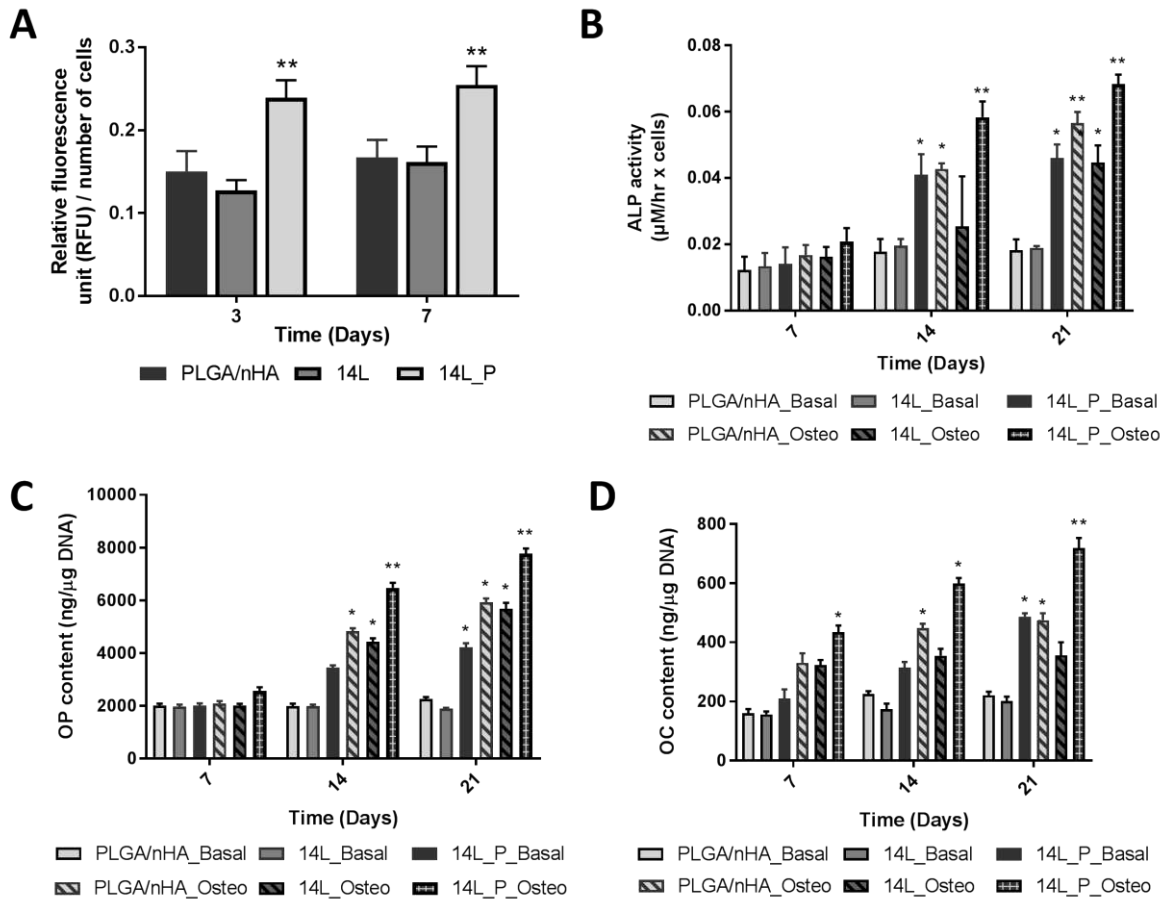
564 **Figure 7.** MicroCT scans (**A-D**, bar= 1 mm) and histological section (**E-H**, bar= 200 µm) of
565 the membranes after testing in vivo rat cranial model: **A,E** No construct, **B,F** Composite
566 membrane, **C,G** Composite membrane functionalised by LbL (14L), **D,H** Composite
567 membrane functionalised by LbL with the peptide sequences grafting (14L_P). For the
568 histological section: ▲- new bone and ●- calvarial bone.
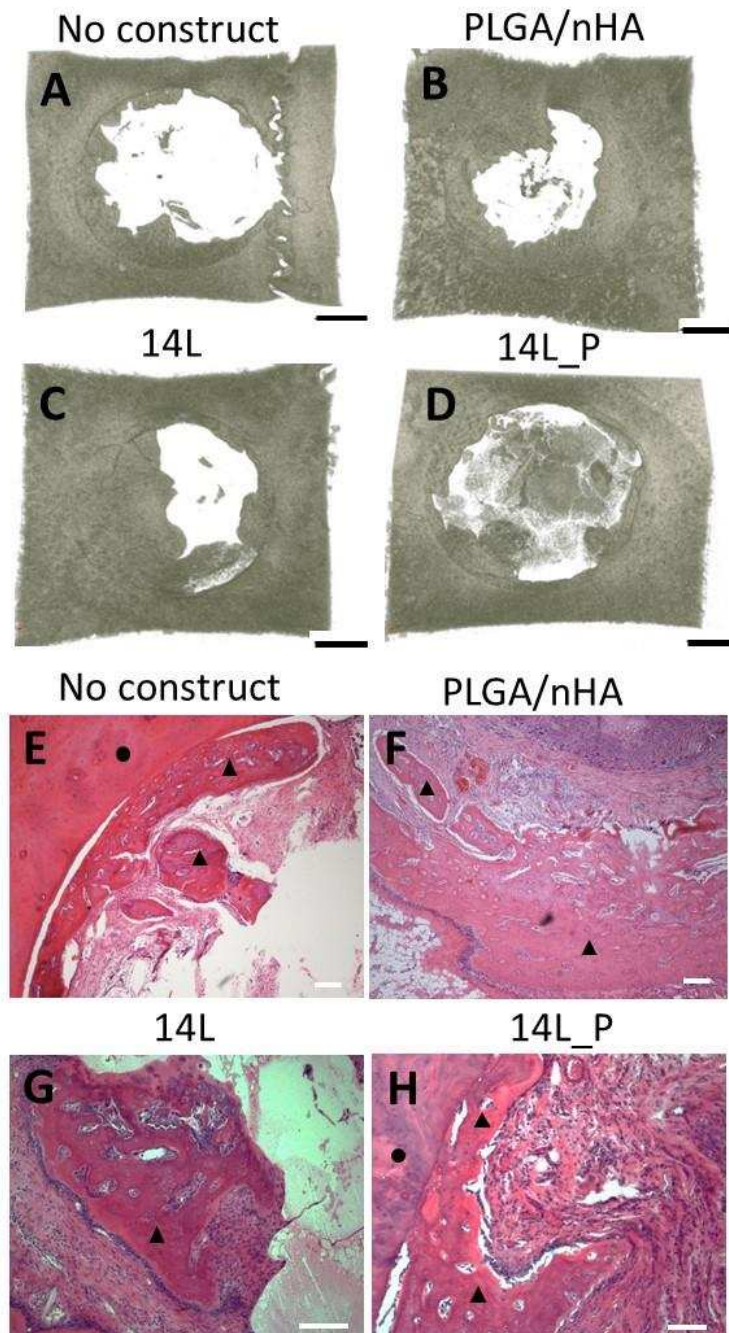
569

570

571 **Table 1.** Atomic concentration (%) of the characteristic elements present in the multilayer and
572 the core-levels of composite membranes after Layer-by-layer assembly.

Sample	C1s (%)	O1s (%)	N1s (%)	S2p (%)	S/N ratio	288.5 eV N-C=O (%)	286.9 eV −C−O− (%)	284.6 eV −C−H−, C−C− (%)
PLGA/nHA_am	66.2±0.3	33.2±0.4	0.6±0.1	-	-	23.5±1.4	31.3±1.8	45.2±2.1
1L	73.9±0.5	25.0±0.3	0.3±0.1	0.8±0.1	0.95±0.16	22.3±1.8	33.7±2.4	44.0±2.8
2L_P	74.1±0.4	23.2±0.3	2.2±0.3	0.4±0.1	0.18±0.25	22.0±1.9	32.8±2.1	45.2±3.4
4L_P	72.6±0.3	23.3±0.4	3.4±0.2	0.7±0.1	0.20±0.18	17.8±2.3	35.0±2.0	47.2±2.5
9L_P	71.9±0.5	20.9±0.4	4.7±0.2	2.5±0.3	0.53±0.31	4.5±1.2	15.0±1.7	79.5±3.1
10L_P	71.7±0.4	20.5±0.3	6.2±0.3	1.6±0.2	0.25±0.23	4.7±1.1	12.3±1.4	83.0±2.3
13L_P	72.0±0.3	20.7±0.2	4.5±0.3	2.8±0.2	0.62±0.22	4.0±1.0	11.4±1.2	84.6±1.9
14L_P	70.9±0.4	20.9±0.3	6.7±0.2	1.5±0.1	0.22±0.18	4.2±1.1	11.8±1.2	84.0±2.4

573

574

575 **The table of contents**

576 **Layer-by-layer (LbL) assembly is a powerful tool to modify the surface of biomedical**
577 **devices for imparting enhanced biological properties.** This work proposed an in vitro
578 model for mimicking the bone healing process, by grafting appropriate bone peptide
579 sequences to the discrete nanolayers for improving the mesenchymal stem cells adhesion,
580 proliferation and differentiation, and the formation of mineralisation matrix.
581
582 **Keywords**: electrospinning, layer-by-layer, osteoconductivity, osteoinductivity, peptides.
583

584 P. Gentile*, A. M. Ferreira. J. T. Callaghan, C. A Miller, J. Atkinson, C. Freeman, P V
585 Hatton*

586
587 **Multilayer nanocoating as in vitro model for bone healing process**
588
589 ToC figure (55 mm broad × 50 mm high)
590
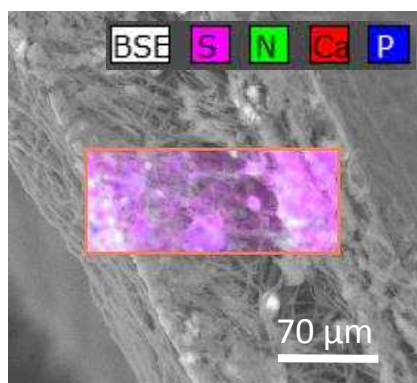
591
592
593

594   **References**
595
596   [1]   L. R. Chaudhary, A. M. Hofmeister, K. A. Hruska, Bone 2004, 34, 402.
597   [2]   B. Bragdon, O. Moseychuk, S. Saldanha, D. King, J. Julian, A. Nohe, Cell Signal 2011,
598   23, 609; A. H. Reddi, Nat Biotechnol 1998, 16, 247.
599   [3]   Z. F. Lu, S. I. Roohani-Esfahani, J. J. Li, H. Zreiqat, Nanomed-Nanotechnol 2015, 11,
600   219; X. Zhang, J. Guo, Y. S. Zhou, G. Wu, Tissue Eng Part B-Re 2014, 20, 84.
601   [4]   Y. W. Chen, F. Ding, H. F. Nie, A. W. Serohijos, S. Sharma, K. C. Wilcox, S. Y. Yin,
602   N. V. Dokholyan, Arch Biochem Biophys 2008, 469, 4; M. Tallawi, E. Rosellini, N. Barbani,
603   M. G. Cascone, R. Rai, G. Saint-Pierre, A. R. Boccaccini, J R Soc Interface 2015, 12,
604   20150254.
605   [5]   A. K. Banga, Therapeutic peptides and proteins: formulation, processing, and delivery
606   systems, CRC press, 2015.
607   [6]   M. D. Pierschbacher, E. Ruoslahti, Nature 1984, 309, 30; R. G. LeBaron, K. A.
608   Athanasiou, Tissue engineering 2000, 6, 85.
609   [7]   P. Gentile, C. Ghione, C. Tonda-Turob, D. M. Kalaskar.
610   [8]   M. Hasenbein, T. T. Andersen, R. Bizios, Biomaterials 2002, 23, 3937.
611   [9]   K. C. Dee, T. T. Andersen, R. Bizios, Journal of biomedical materials research 1998,
612   40, 371.
613   [10]   A. Rezania, K. E. Healy, Biotechnology progress 1999, 15, 19; P. Gentile, C. Ghione,
614   C. Tonda-Turo, D. M. Kalaskar, RSC Advances 2015, 5, 80039; G. M. Harbers, K. E. Healy,
615   Journal of Biomedical Materials Research Part A 2005, 75, 855.
616   [11]   M. Schuler, D. W. Hamilton, T. P. Kunzler, C. M. Sprecher, M. de Wild, D. M.
617   Brunette, M. Textor, S. G. P. Tosatti, Journal of Biomedical Materials Research Part B:
618   Applied Biomaterials 2009, 91, 517.
619   [12]   C. D. Reyes, A. J. García, Journal of Biomedical Materials Research Part A 2003, 65,
620   511.
621   [13]   A. M. Wojtowicz, A. Shekaran, M. E. Oest, K. M. Dupont, K. L. Templeman, D. W.
622   Hutmacher, R. E. Guldberg, A. J. García, Biomaterials 2010, 31, 2574.
623   [14]   K. G. Sreejalekshmi, P. D. Nair, Journal of biomedical materials research Part A 2011,
624   96, 477.
625   [15]   A. A. Sawyer, K. M. Hennessy, S. L. Bellis, Biomaterials 2007, 28, 383; H. Shin, S. Jo,
626   A. G. Mikos, Biomaterials 2003, 24, 4353.
627   [16]   X. He, J. Ma, E. Jabbari, Langmuir 2008, 24, 12508; H. Shin, K. Zygourakis, M. C.
628   Farach‐Carson, M. J. Yaszemski, A. G. Mikos, Journal of Biomedical Materials Research
629   Part A 2004, 69, 535.
630   [17]   P. Gentile, I. Carmagnola, T. Nardo, V. Chiono, Nanotechnology 2015, 26, 422001; A.
631   A. Mamedov, N. A. Kotov, Langmuir 2000, 16, 5530.
632   [18]   Z. Tang, Y. Wang, P. Podsiadlo, N. A. Kotov, Advanced materials 2006, 18, 3203.
633   [19]   P. Gentile, M. E. Frongia, M. Cardellach, C. A. Miller, G. P. Stafford, G. J. Leggett, P.
634   V. Hatton, Acta biomaterialia 2015, 21, 35.
635   [20]   B. Zhou, X. Jin, J. Li, W. Xu, S. Liu, Y. Li, B. Li, RSC Advances 2014, 4, 54517.
636   [21]   Y. Hu, K. Cai, Z. Luo, R. Zhang, L. Yang, L. Deng, K. D. Jandt, Biomaterials 2009,
637   30, 3626.
638   [22]   P. Podsiadlo, S. Paternel, J.-M. Rouillard, Z. Zhang, J. Lee, J.-W. Lee, E. Gulari, N. A.
639   Kotov, Langmuir 2005, 21, 11915.
640   [23]   C. Tonda-Turo, E. Cipriani, S. Gnavi, V. Chiono, C. Mattu, P. Gentile, I. Perroteau, M.
641   Zanetti, G. Ciardelli, Materials Science and Engineering: C 2013, 33, 2723.
642   [24]   S. Gnavi, B. E. Fornasari, C. Tonda-Turo, G. Ciardelli, M. Zanetti, I. Perroteau, S.
643   Geuna, "The influence of electrospun fibre diameter on Schwann cell behavior and axonal

644 outgrowth", presented at JOURNAL OF TISSUE ENGINEERING AND REGENERATIVE
645 MEDICINE, 2014.
646 [25]   J. R. Woodard, A. J. Hilldore, S. K. Lan, C. J. Park, A. W. Morgan, J. A. C. Eurell, S.
647 G. Clark, M. B. Wheeler, R. D. Jamison, A. J. W. Johnson, Biomaterials 2007, 28, 45.
648 [26]   V. Milleret, B. Simona, P. Neuenschwander, H. Hall, Eur Cell Mater 2011, 21, 286.
649 [27]   E. Fortunati, S. Mattioli, L. Visai, M. Imbriani, J. L. G. Fierro, J. M. Kenny, I.
650 Armentano, Biomacromolecules 2013, 14, 626.
651 [28]   M. Nitschke, G. Schmack, A. Janke, F. Simon, D. Pleul, C. Werner, Journal of
652 biomedical materials research 2002, 59, 632.
653 [29]   J. L. Vickery, A. J. Patil, S. Mann, Advanced Materials 2009, 21, 2180.
654 [30]   N. P. Camacho, P. West, P. A. Torzilli, R. Mendelsohn, Biopolymers 2001, 62, 1.
655 [31]   C. Vidal, W. Li, B. Santner‐Nanan, C. K. Lim, G. J. Guillemin, H. J. Ball, N. H.
656 Hunt, R. Nanan, G. Duque, Stem Cells 2015, 33, 111.
657 [32]   S. Zhou, J. S. Greenberger, M. W. Epperly, J. P. Goff, C. Adler, M. S. LeBoff, J.
658 Glowacki, Aging cell 2008, 7, 335.
659 [33]   M. E. Santocildes‐Romero, A. Crawford, P. V. Hatton, R. L. Goodchild, I. M.
660 Reaney, C. A. Miller, Journal of tissue engineering and regenerative medicine 2015, 9, 619.
661 [34]   L. Hao, J. Lawrence, Laser Surface Treatment of Bio-Implant Materials, 11.
662 [35]   S. Sun, W. Yu, Y. Zhang, F. Zhang, Journal of Materials Science: Materials in
663 Medicine 2013, 24, 1079.
664 [36]   A. Sabokbar, P. J. Millett, B. Myer, N. Rushton, Bone and mineral 1994, 27, 57.
665 [37]   J. Sodek, J. Chen, T. Nagata, S. Kasugai, R. Todescan, I. W. S. Li, R. H. Kim, Annals
666 of the New York Academy of Sciences 1995, 760, 223.
667 [38]   S. Bose, M. Roy, A. Bandyopadhyay, Trends in biotechnology 2012, 30, 546.
668 [39]   R. J. Kohal, M. Bächle, W. Att, S. Chaar, B. Altmann, A. Renz, F. Butz, Dental
669 Materials 2013, 29, 763.
670 [40]   S. Liao, W. Wang, A. Yokoyama, Y. Zhu, F. Watari, S. Ramakrishna, C. K. Chan,
671 Journal of Bioactive and Compatible Polymers 2010; J. M. Song, S. H. Shin, Y. D. Kim, J. Y.
672 Lee, Y. J. Baek, S. Y. Yoon, H. S. Kim, International journal of oral science 2014, 6, 87.
673 [41]   A. A. Sawyer, S. J. Song, E. Susanto, P. Chuan, C. X. Lam, M. A. Woodruff, D. W.
674 Hutmacher, S. M. Cool, Biomaterials 2009, 30, 2479.
675 [42]   J. T. Schantz, D. W. Hutmacher, C. X. Lam, M. Brinkmann, K. M. Wong, T. C. Lim,
676 N. Chou, R. E. Guldberg, S. H. Teoh, Tissue Eng 2003, 9 Suppl 1, S127; J. T. Schantz, S. H.
677 Teoh, T. C. Lim, M. Endres, C. X. Lam, D. W. Hutmacher, Tissue Eng 2003, 9 Suppl 1, S113.
678 [43]   C. Vaquette, W. Fan, Y. Xiao, S. Hamlet, D. W. Hutmacher, S. Ivanovski,
679 Biomaterials 2012, 33, 5560.
680 [44]   P. Gentile, C. J. Wilcock, C. A. Miller, R. Moorehead, P. V. Hatton, Materials 2015, 8,
681 2297.
682
683

685

686   Supporting Information

687

688

689   **Multilayer nanoscale encapsulation of biofunctional peptides to enhance bone tissue**
690   **regeneration in vivo.**
691   Piergiorgio Gentile* and Paul V Hatton*

692

693   Methods

694   For the morphological evaluation, after 6 days of culturing period, samples were washed with

695   PBS and fixed with 4 % formalin solution (0.5 mL) for 15 min at room temperature (RT). The

696   cells were washed with PBS, containing 0.2 % Triton X, for 2 min. After the fixation and

697   permeation steps, cells were washed again and stained with 4,6-Diamidino-2-phenyindole

698   dilactate (1:1000 DAPI, Sigma-Aldrich) for 2 min at RT, and Phalloidin-

699   Tetramethylrhodamine B isothiocyanate (10 µM phalloidin Sigma-Aldrich) for 1 h at RT.

700   Finally, cells were washed and observed with the help of Axioplan 2 imaging fluorescent

701   microscope with a digital camera QIC AM 12-bit (Zeiss).

702

703   Figures

704   **Figure S1.** SEM micrograph of the electrospun membranes after Layer-by-layer surface

705   modification with the obtainment of 20 nanolayers. Bar= 10µm.
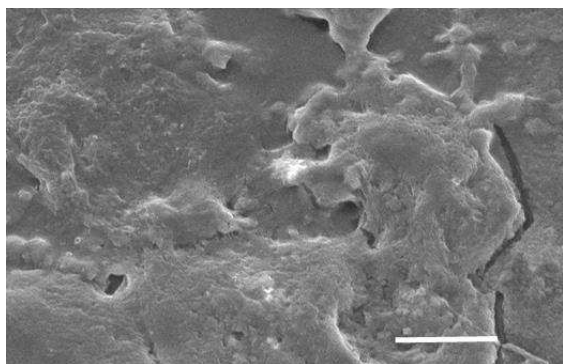

706

707

708

709

710

711   **Figure S2.** (**A**) BM-MSCs metabolic activity (PrestoBlue® assay) after culturing for 3 and 7

712   days and (**B**) Intracellular alkaline phosphatase activity of BM-MSCs (Alkaline Phosphatase

713   detection kit –Sigma Aldrich Alkaline phosphatase assay kit (APF-1KT)) after culturing

714   either with basal or osteogenic media for 7, 14 and 21 days on LbL functionalised membranes

715   with the single peptide sequence (* $p < 0.05$).
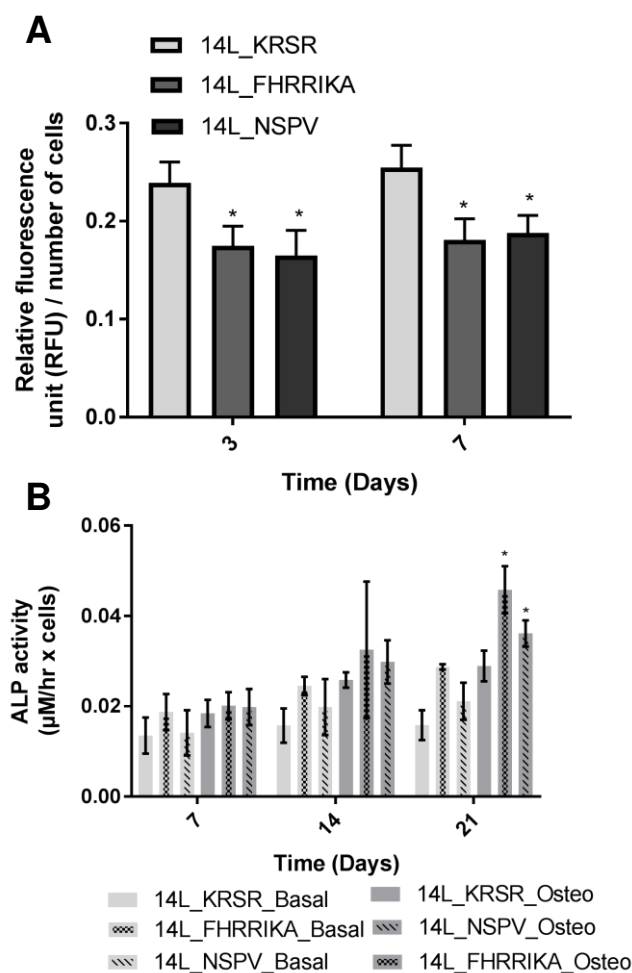
716

717

718 **Figure S3.** Fluorescence microscopy of composite membranes after 7 days of culture on: (a)

719 PLGA/nHA membrane; (b) 14L membrane and (c) 14L_P membrane. DAPI in blue colour

720 and stains nucleus of cells; Phalloidin in green colour and stains the actin filamentous.

721

722
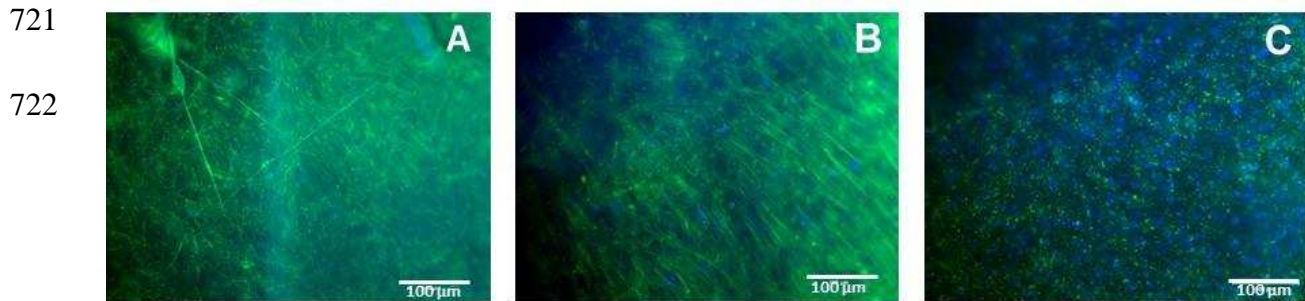
723 **Movie S1-4.** Micro-CT 3D reconstruction movies of 4.5mm Ø defects in the crania of Wistar

724 rats after 4 weeks of implantation:

725   **Movie S1**: Sham

726   **Movie S2**: PLGA/nHA membrane

727   **Movie S3**: 14L membrane

728   **Movie S4**:14L_P membrane